Frontiers of Physics
https://doi.org/10.1007/s11467-019-0916-1
Front. Phys.
14(6), 63601 (2019)

RESEARCH ARTICLE

Influence of surface charges on the emission polarization properties of single CdSe/CdS dot-in-rods

Guo-Feng Zhang[1,†], Chang-Gang Yang[1], Yong Ge[2], Yong-Gang Peng[3,‡], Rui-Yun Chen[1], Cheng-Bing Qin[1], Yan Gao[1], Lei Zhang[1], Hai-Zheng Zhong[2], Yu-Jun Zheng[3], Lian-Tuan Xiao[1,*], Suo-Tang Jia[1]

[1] *State Key Laboratory of Quantum Optics and Quantum Optics Devices, Institute of Laser Spectroscopy, and Collaborative Innovation Center of Extreme Optics, Shanxi University, Taiyuan 030006, China*
[2] *Beijing Key Laboratory of Nanophotonics and Ultrafine Optoelectronic Systems, School of Materials Science and Engineering, Beijing Institute of Technology, Beijing 100081, China*
[3] *School of Physics, Shandong University, Jinan 250100, China*
*Corresponding authors. E-mail: †guofeng.zhang@sxu.edu.cn, ‡ygpeng@sdu.edu.cn, *xlt@sxu.edu.cn*
Received May 17, 2019; accepted June 27, 2019

We report an experimental investigation of the influence of surface charges on the emission polarization properties of single CdSe/CdS dot-in-rods (DRs), which is important for their polarization-based practical applications. By covering the single DRs with N-type semiconductor indium tin oxide (ITO) nanoparticles, the surface of single DRs is charged by ITO through interfacial electron transfer. This is confirmed by the experimental observations of the reduced photoluminescence intensities and lifetimes as well as the suppressing blinking. It is found that the full width at half maximum of histogram of polarization degrees of the single DRs is broadened from 0.24 (on glass) to 0.41 (in ITO). In order to explain the exprimental results, the band-edge exciton fine structure of single DRs is calculated by taking into account the sample parameters, the emission polarization, and the surface charges. The calculation results show that the level ordering of the emitting states determines the polarization degrees tending to increase or decrease under the influence of surface electrons. The surface electrons can induce an increase in the spacing between the emitting levels to change the populations and thus change the polarization degrees. In addition, different numbers of surface electrons may randomly distribute on the long CdSe/CdS rods, leading to the heterogeneous influences on the single DRs causing the broadening of polarization degrees also.

Keywords single CdSe/CdS dot-in-rods, polarization properties, surface charges, band-edge exciton fine structure

1 Introduction

Colloidal semiconductor nanocrystals have been extensively applied to a variety of optoelectronic devices, such as light-emitting diodes [1, 2], lasers [3], detectors [4], single photon sources [5], and photovoltaics [6], due to their widely tunable optoelectronic properties with the size, shape, and composition [7–14]. The heterostructured CdSe/CdS dot-in-rods (DRs) have been considered to be one of the most promising types of nanocrystals for optoelectronic applications in the visible spectral range at room temperature [15, 16]. The CdSe/CdS DRs are made by growing a rod-shaped CdS shell around a nearly spherical CdSe core [17], which have many excellent properties, such as improved photoluminescence (PL) quantum yields [18], enhanced optical gain [19–21], and larger two-photon absorption cross section [22]. Moreover, the DRs have additional interesting features: linearly polarized band-edge absorption and emission. A high degree of emission polarization along the axis of the CdS rod has been observed and investigated [23–30]. It has been demonstrated that the linearly polarized emission in the CdSe/CdS DRs depends on the elongated shape of the CdS rods, the prolate CdSe core as well as the large core size [26, 27]. Furthermore, the emission polarization has been confirmed to be related to the fine structure splitting of band-edge exciton, the levels ordering and the oscillator strengths of the various transitions [23, 26, 27].

Recently, spectral diffusion in the single CdSe/CdS DRs was observed and investigated by combined experimental and theoretical analysis, which was attributed to fluctuations of the surface charges of DRs [31–34]. The surface charges can change the squared electron and hole wave

function overlap and thereby modify the exciton emission energy of DRs [33, 34]. The influence of surface charges on the spectral diffusion was also observed in the conventional spherical CdSe quantum dots (QDs) [35–38]. The possible origin of the surface charges was speculated to be from the photogenerated charges or the surface ligand layer [33, 39]. However, the surface electrons of QDs can come from the N-type semiconductor indium tin oxide (ITO) nanoparticles by interfacial electron transfer [40–44]. The electrons at single QD surface from ITO could result in the spectral peak emission energies to show a red shift as large as approximately −35 meV with respect to that on glass coverslip [40]. Besides the spectral shift, the surface electrons from ITO also modify the photon emission statistics [42, 44], reduce the PL lifetimes and suppress the PL blinking dynamics [41, 43]. Moreover, the surface electrons also induce a linear polarization property of single CdSe QDs at room temperature, which was attributed to the surface electrons inducing a significant Stark distortion of the electron and hole wave functions [37, 45, 46]. In the CdSe/CdS DRs based optoelectronic devices, the surface charges of DRs always exist due to the interfacial charge transfer between the DRs and other materials [47]. It has been of great interest to clarify the influence of surface charges on the polarization properties, however, has not been investigated yet.

Here, we investigate the influence of surface charges on the emission polarization properties of single CdSe/CdS DRs. When single DRs are covered with N-type semiconductor ITO nanoparticles, the surface of single DRs is charged by ITO through interfacial electron transfer, which is further confirmed by the reduced PL intensities and lifetimes as well as the suppressed PL blinking. The emission polarization properties of single DRs are measured by single particle polarization microscopy. Compared with that on glass coverslips, a broadened histogram of polarization degrees is observed for single DRs in ITO. We attribute the broadened behavior to the influence of surface electrons on the electron and hole wave functions of DRs. Since the polarization degrees are determined by band-edge exciton fine structure which relates to the electron and hole wave functions, we further calculate the band-edge exciton fine structure to explain the broadening behavior.

2 Results and discussion

2.1 PL properties of single DRs

Figure 1(a) presents a transmission electron microscopy (TEM) image of the CdSe/CdS DRs. The absorption and emission spectra of DRs are shown in Fig. 1(b), where the PL peak locates at ∼ 608 nm. Schematic representation of the sample preparation for single DRs in ITO is depicted in Fig. 1(c). Detailed information about sample preparation can be found in the Methods. Briefly, the single DRs in toluene were spin-coated onto glass coverslip and then the ITO nanoparticles were spin-coated onto individual DRs. Through these processes, the individual DRs are in contact with ITO nanoparticles. The scanning electron microscope image of spin-coated ITO nanoparticles is presented in Fig. 1(d). The N-type ITO nanoparticles with a high electron density of $\sim 2.2 \times 10^{21}$ cm^{-3} have a higher Fermi level than that of the DRs, and thus the ITO can be utilized as an electron donor to charge for the DRs [41, 48]. Scheme of the experimental setup for single particle polarization measurement is presented in Fig. 2(a). The experimental setup has been used to measure single-particle polarization in our previous works [46, 49]. Details about the experimental setup and the measurement process are presented in the Methods. In order to reduce the

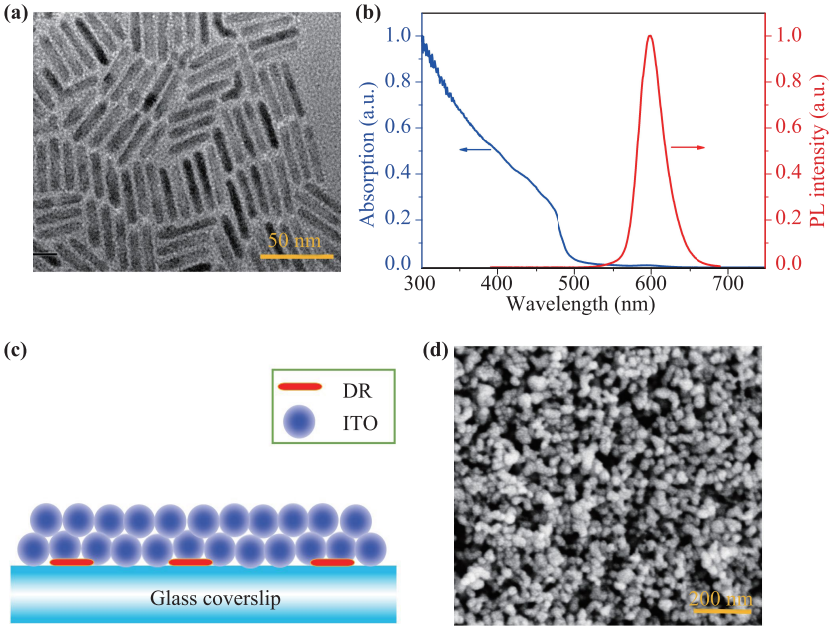

Fig. 1 Schematic representation of sample preparation and material characteristics. **(a)** Transmission electron microscope image of CdSe/CdS dot-in-rods (DRs). **(b)** Absorption and emission spectra of DRs in solution. **(c)** The schematic of single DRs covered with indium tin oxide (ITO) nanoparticles film. **(d)** Scanning electron microscope image of the ITO nanoparticles film.

effects of the trion states on the degrees of polarization of single DRs [50], the pump fluence was set at $\langle N \rangle = 0.1$ as a weak excitation condition [44, 51], where $\langle N \rangle$ represents the average number of photons absorbed per DR per pulse. All measurements were performed at room temperature.

The typical PL trajectories of single DRs on glass and in ITO are recorded by the confocal microscope with an integration time of 10 ms, as presented in Fig. 2(b). The histograms of PL intensities (on level) for $\sim$ 100 single DRs on glass and in ITO, as shown in Fig. S1 in the Supplementary Materials (SM), are fitted by Gauss functions with mean values and standard deviations to be 394 ± 134 and 253 ± 111 counts/10ms, respectively. Therefore, single DRs in ITO have a lower PL intensity than that on glass, which are similar to the previous reports for single CdSe/ZnS QDs in ITO [41–44]. Blinking behaviors can be found in the PL trajectories due to the activation and deactivation of surface trap states which is confirmed by linear fluorescence lifetime-intensity distribution (FLID) in Fig. S2 in SM [52–54]. Note that the single DRs in ITO have less PL blinking than that on glass, as will be analyzed and discussed later. A typical second-order correlation function [$g^{(2)}$] curve with a low value of $g^{(2)}(0)$ [Fig. 2(c)] indicates that the observed PL emission originates from an individual DR [55]. A typical PL decay curve of single DRs in ITO and corresponding exponential fit are presented in Fig. 2(d). Histograms of single exciton lifetimes obtained from exponential fitting for single DRs on glass and in ITO, as shown in Fig. 3(a), are fitted by Gauss functions with average values and standard deviations to be 21.6 ± 5.8 ns and 16.5 ± 7.5 ns, respectively. Therefore, single DRs in ITO have a shorter lifetime than that on glass, which was attributed to exciton Auger recombination and hole transfer processes involving the additional surface electrons [41].

We analyze the blinking dynamics of single DRs in ITO and on glass by calculating on- and off-state probability densities $P_{\rm on}(t)$ and $P_{\rm off}(t)$ (see SM for details). Both $P_{\rm on}(t)$ and $P_{\rm off}(t)$ of single QDs in the two cases show a power law distribution, as shown in Fig. 3(b). By analyzing $P_{\rm on}(t)$ and $P_{\rm off}(t)$ of $\sim$ 100 single DRs on glass and in ITO (see SM), it can be found that single DRs in ITO have a smaller $\langle \alpha_{\rm on} \rangle$ but a larger $\langle \alpha_{\rm off} \rangle$ than that on glass, indicating increased probability densities of long on-state events and reduced probability densities of long off-state events. Therefore, the PL blinking of single DRs in ITO is suppressed due to the interfacial electron transfer from ITO to single DRs which removes the surface trap states and the valence band holes of single DRs [41, 43]. The observation of blinking suppression of single nanocrystals was also generally used to confirm if the interfacial electron transfer occurs between nanocrystals and other materials [56, 57]. Overall, for the single DRs in ITO, the observed decreasing of PL intensities and lifetimes as well as the suppressing of PL blinking are consistent with the results of single CdSe/ZnS QDs in ITO [41–44], which can further confirm the fact that the surface of single DRs is charged by ITO nanoparticles.

2.2 Polarization measurements for single DRs

The polarization measurement was performed by single particle polarization microscopy based on emission polar-

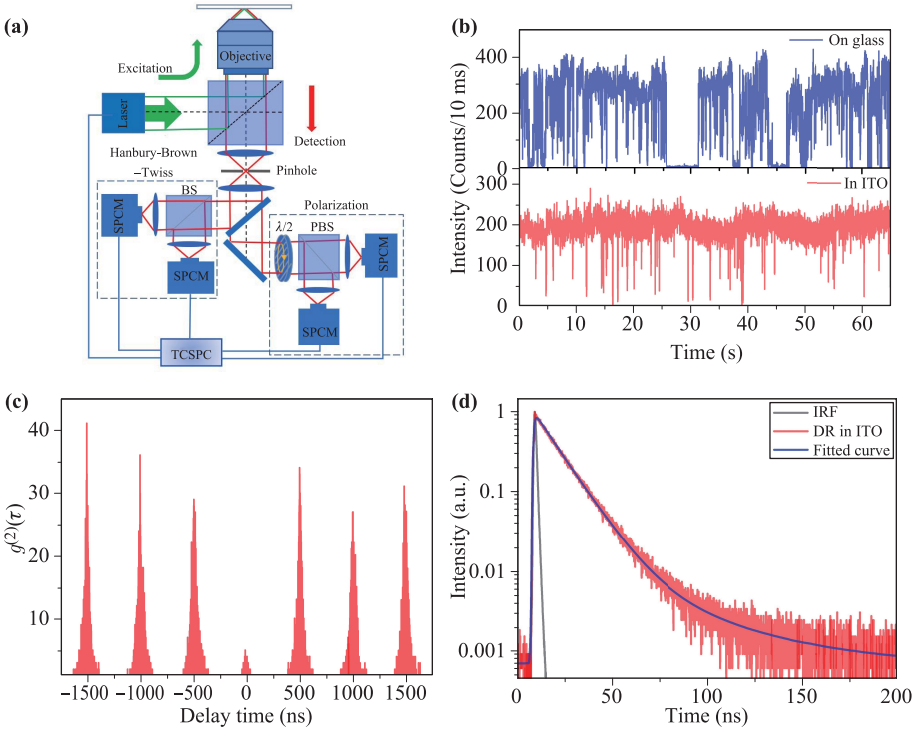

Fig. 2 Schematic of experimental setup and photoluminescence (PL) properties of single DRs. **(a)** Scheme of the experimental setup for single particle polarization measurement. **(b)** Typical PL intensity trajectories for single DRs on glass and in ITO, respectively. **(c)** Typical second-order correlation curve of single DRs in ITO. **(d)** Typical PL decay curve and corresponding exponential fit for single DRs in ITO. IRF indicates the instrument response function of system.

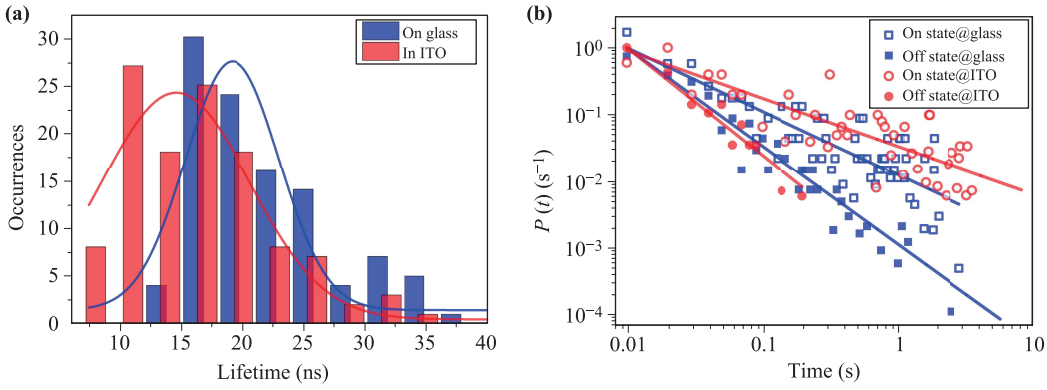

Fig. 3 **(a)** Histograms of PL lifetimes for the single DRs on glass and in ITO, respectively. **(b)** Normalized probability densities of on-states $[P_{\rm on}(t)]$ and off states $[P_{\rm off}(t)]$ for single DRs on glass and in ITO, respectively. The solid lines are well fits with the power laws, $P_i(t) = A_i t^{-\alpha_i} (i = \text{on or off})$. Fitting parameters: on glass $\alpha_{\rm on} = 0.95$, $\alpha_{\rm off} = 1.47$; in ITO $\alpha_{\rm on} = 0.71$, $\alpha_{\rm off} = 1.60$.

ization analysis in the far field [26, 46, 58]. The rotating half-wave plate combined with the polarizing beamsplitter cube was used to measure the polarization degree of single DRs. When the polarization direction of linearly polarized photons from single DRs rotates with the rotation of the half-wave plate, the polarizing beamsplitter cube splits horizontal and vertical polarized photons into two single photon detectors respectively. A typical PL intensity trajectory as a function of the half-wave plate angle is shown in Fig. 4(a). Note that when the half-wave plate rotates from 0° to 180°, the linearly polarized photons rotate from 0° to 360° and thus there are two modulation cycles for single DR's emission. The polarization degree p is defined by $p = (I_{\max} - I_{\min})/(I_{\max} + I_{\min})$, where $I_{\max}$ and $I_{\min}$ are the maximum and minimum photon counts of one of detectors in an emission modulation cycle. $I_{\max}$ and $I_{\min}$ can be obtained by fitting the PL intensity trajectory with the equation, $I(\theta_{\lambda/2}) = (I_{\max} - I_{\min})\cos^2(\theta_{\lambda/2}) + I_{\min}$ [blue curve in Fig. 4(a)] [58], where $\theta_{\lambda/2}$ is the angle of the half-wave plate. Based on the fitting values of $I_{\max}$ and $I_{\min}$, the polarization degree p of 0.44 is obtained for the PL intensity trajectory shown in Fig. 4(a). An average background has been subtracted from the trajectory before fitting, but the fitting error always exists due to the inhomogeneity of background and PL blinking.

We have investigated more than 220 single DRs on glass and in ITO respectively, and histograms of the polarization degrees are shown in Figs. 4(b) and (c), respectively. The histograms were fitted by Gaussian functions to give average polarization degrees with standard deviations to be 0.39 ± 0.10 (on glass) and 0.40 ± 0.17 (in ITO), respectively. Although the average polarization degrees are approximately equal in the two cases, the full width at half maximum (FWHM) of the histogram for the single DRs in ITO (~ 0.41) is broader than that on glass (~ 0.24). It has been reported that the surface charges can strongly affect the electron–hole wave functions which relate to band-edge exciton fine structure [26, 59], and that the band-edge exciton fine structure determines the polarization degrees of single DRs [26]. Therefore, the broadened histogram of that in ITO is correlated with the surface electron effects.

2.3 Band-edge exciton fine structure for single DRs in the two cases

In order to further explain the broadening behavior, we investigate the influence of surface electrons on the band-edge exciton fine structure by using the theoretical approach of Refs. [26, 59]. In CdSe nanocrystals, the band-edge exciton consists of the $1S_{1/2}$ electron and the $1S_{3/2}$ hole. The electron with spin of 1/2 and the hole with spin of 3/2 have 2 and 4 possible spin projections, respectively, so the band-edge exciton fine structure comprises eight states: $|\pm 2\rangle$, $|\pm 1^{\rm L}\rangle$, $|\pm 1^{\rm U}\rangle$, $|0^{\rm L}\rangle$, and $|0^{\rm U}\rangle$ [59]. At room temperature the emission of CdSe nanocrystals is a mixture of five bright states: the $|0^{\rm U}\rangle$ state and the degenerate $|\pm 1^{\rm L}\rangle$, $|\pm 1^{\rm U}\rangle$ states. The $|0^{\rm U}\rangle$ state emits linearly polarized photons, and it is a linear 1D dipole that oscillates along the c-axis of the crystal. The $|\pm 1^{\rm L}\rangle$ and $|\pm 1^{\rm U}\rangle$ states are degeneracy 2D dipoles, which are two linear dipoles perpendicularly oscillating inside a plane perpendicular to the c-axis of the crystal. Here the emission of the 1D dipole and the 2D dipoles is collected by a NA = 1.3 objective lens. Considering the large numerical aperture of the objective lens, the polarization degree p is written as [26]

$$p = \left| \frac{p_{1\rm D} I_{1\rm D} - p_{2\rm D} I_{2\rm D}}{I_{1\rm D} + I_{2\rm D}} \right|, \tag{1}$$

where $I_{1\rm D}$ and $I_{2\rm D}$ are the emission probability of the 1D dipole and the 2D dipoles respectively, and $p_{1\rm D}$ and $p_{2\rm D}$ are correction factors to be equal to 1.0 and 0.43 which are gotten by the calculation method given in Ref. [59] for our objective lens.

According to the theory in Ref. [59], we calculate the emission probabilities of the 1D dipole and 2D dipoles, $I_{1\rm D}$ and $I_{2\rm D}$. In the fine structure energy levels, the energy,

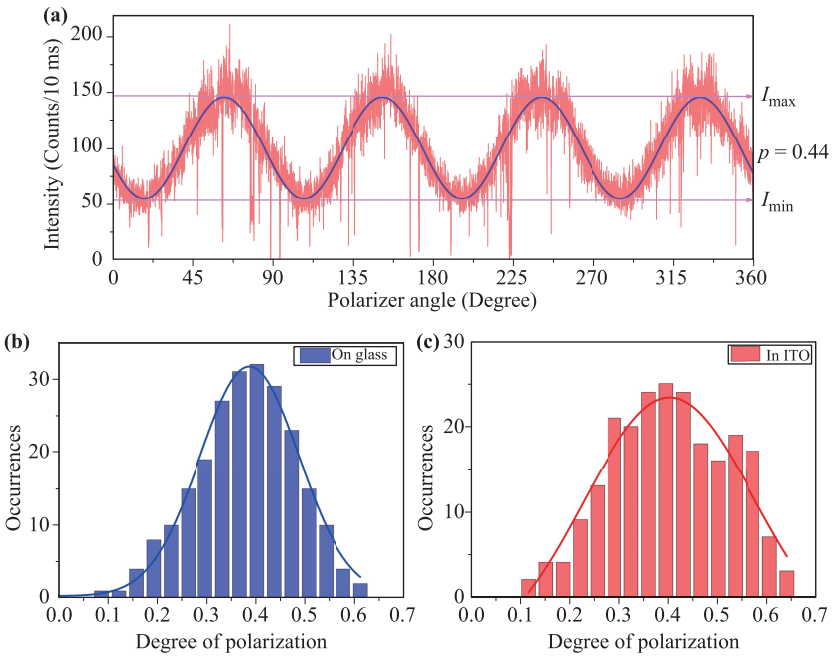

Fig. 4 **(a)** Polarization trajectory for a typical single DR in ITO, and the PL intensity from one of single photon detectors (red line) is plotted as a function of the half-wave plate angle. The trajectory is fitted by $I(\theta_{\lambda/2}) = (I_{\max} - I_{\min})\cos^2(\theta_{\lambda/2}) + I_{\min}$ function to derive the degree of polarization (p). **(b)** Histogram of the values of p for 230 DRs on glass, and the full width at half maximum (FWHM) of the histogram is 0.24. **(c)** Histogram of the values of p for 228 DRs in ITO, and the FWHM of the histogram is 0.41.

ordering and oscillator strength depend on the electron-hole exchange interaction η and the net-splitting Δ between the heavy-hole and light-hole valence sub-bands of the CdSe core. Therefore, the emission probability of a state can be expressed as $I(\eta,\Delta) = N(\eta,\Delta)f(\eta,\Delta)$, where $N(\eta,\Delta)$ is the population of the state at a given temperature, and $f(\eta,\Delta)$ is the oscillator strength. The $N(\eta,\Delta)$ and $f(\eta,\Delta)$, as functions of η and Δ, can be calculated from Ref. [59]. For the 1D dipole emission,

$$I_{1D}(\eta,\Delta) = I_{0^U}(\eta,\Delta) = N_{0^U}(\eta,\Delta)f_{0^U}(\eta,\Delta), \tag{2}$$

and for the 2D dipoles emission,

$$\begin{aligned} I_{2D}(\eta,\Delta) &= I_{+1^U}(\eta,\Delta) + I_{+1^L}(\eta,\Delta) \\ &= 2[N_{+1^U}(\eta,\Delta)f_{+1^U}(\eta,\Delta) \\ &\quad + N_{+1^L}(\eta,\Delta)f_{+1^L}(\eta,\Delta)]. \end{aligned} \tag{3}$$

In addition, the polarization of single DRs also depends on the geometrical shape of CdS shell which induces a dielectric effect to enhance the oscillator strength of the 1D dipole transition [60]. Therefore, the oscillator strength of 1D dipole transition should be multiplied by local field factors R_e [61]. Eq. (2) can be further rewritten as

$$I_{1D}(\eta,\Delta,R_e) = I_{0^U}(\eta,\Delta) = R_e \times N_{0^U}(\eta,\Delta)f_{0^U}(\eta,\Delta). \tag{4}$$

Here, we calculate the local field factors R_e according to the calculation method given in Ref. [52]. The TEM image of CdSe/CdS DRs in Fig. 1(a) shows the aspect ratio of 5, which yields R_e of 2.4.

Using the theory of Ref. [59], we calculated the polarization degree p by Eq. (1) as a function of the parameters η and Δ. The curves of polarization degrees as a function of η and Δ is shown in Fig. 5(a). For obtaining the exact value of Δ, we firstly estimate η by the expression $\eta = \left(\frac{a_{ex}}{a}\right)^3 \hbar\omega_{ST}\chi(\beta)$ [59], where exciton Bohr radius $a_{ex} = 56$ Å, our CdSe core radius $a = 14.5$ Å, the bulk exchange splitting value $\hbar\omega_{ST} = 0.13$ meV, and $\chi(\beta) \approx 0.78$. $\chi(\beta)$ is a size-independent dimensionless function related to electron-hole wave function overlap [59]. Therefore, η is estimated to be ~ 5.8 meV for our DRs sample. According to the value of η and the measured polarization degrees, the net-splitting Δ can be determined by Fig. 5(a). In the figure, the red line of $\eta = 5.8$ meV intersects with the curves of polarization degrees, and the intersections marked with the green circles can indicate the values of Δ for various polarization degrees.

It has been reported that the surface charges can strongly decrease the overlap of electron and hole wave function [33, 34] and that both the electron-hole exchange interaction η and the net-splitting Δ depend on the electron-hole wave functions [59, 62]. Therefore, the surface charges are able to change the values of η and Δ. The changes of the parameters η and Δ under the influence of the surface electrons were estimated in the SI. The results of estimation are marked with red stars in Fig. 5(a) which indicate the values η and Δ as well as the corresponding values of p. From the figure, it is found that the value of η was reduced under the influence of the surface electrons, and the values of Δ were increased toward negative and larger values and the corresponding p were increased for $p > 0.35$, while the values of Δ were increased toward positive and larger values but the corresponding p were reduced for $p < 0.35$. For example, the values of $p = 0.40$, 0.50 and 0.60 are increased to $p = 0.41$, 0.54 and 0.65, while the values of $p = 0.15$ and 0.25 are reduced to $p = 0.10$ and 0.23, respectively. Therefore, both the increase and the decrease of the polarization degrees broaden the histogram from the middle to both sides.

Band-edge exciton fine structure of single DRs was deduced by taking into account the sample parameters, the

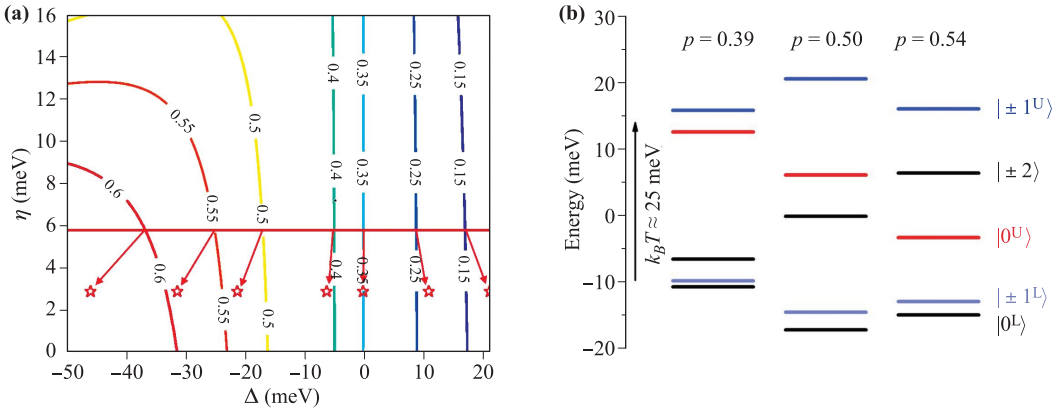

Fig. 5 Calculated polarization degree p and band-edge exciton fine structure. **(a)** The polarization degree p as a function of the net-splitting Δ and the electron–hole interaction η for local field factors R_e of 2.4. The green circles in the figure indicate the values of p and the corresponding parameters of η and Δ without considering the influence of the surface electrons, and the red stars indicate the values of η and Δ as well as corresponding p under the influence of the surface electrons. **(b)** Band-edge exciton fine structure deduced by taking into account the sample parameters, the emission polarization and the surface electrons. Examples of the band-edge exciton fine structure calculated for three typical values of p. The band-edge exciton fine structures for $p = 0.39$ and 0.50 without considering the influence of surface electrons. The band-edge exciton fine structure of $p = 0.50$ is changed into that of $p = 0.54$ under the influence of surface electrons. The thermal energy at 290 K is ~25 meV.

emission polarization and the surface electrons. Figure 5(b) presents the band-edge exciton fine structure levels for the three typical polarization degrees of 0.39, 0.50, and 0.54 using the values of η and Δ from Table 1. The exciton fine structures for polarization degrees of 0.39 and 0.50 were derived without considering the influence of surface electrons. When considering the influence of surface electrons, the band-edge exciton fine structure of $p = 0.50$ is changed into that of $p = 0.54$. We can see from the figure that the change of exciton fine structure is very obvious. In Table 1, we give the exciton fine structure and emission parameters for the three polarization degrees. Note that the $|\pm 1^{\mathrm{L}}\rangle$ state has a much smaller oscillator strength than that of the other states, it therefore makes less contribution to polarization degree. So, we mainly compare the populations and the oscillator strengths between the $|0^{\mathrm{U}}\rangle$ and $|\pm 1^{\mathrm{U}}\rangle$ states to understand the polarization changes. The $|0^{\mathrm{U}}\rangle$ and $|\pm 1^{\mathrm{U}}\rangle$ levels are highlighted in red and blue in the band-edge exciton fine structures in Fig. 5(b) and Fig. S3 in SM. As mentioned above, the $|0^{\mathrm{U}}\rangle$ state is a linear 1D dipole to make contribution to the linear polarization, while $|\pm 1^{\mathrm{U}}\rangle$ states are degeneracy 2D dipoles to reduce the linear polarization. By comparing the band-edge exciton fine structures of different polarization degrees in Fig. 5(b) and Fig. S3, it is found that the level ordering of $|0^{\mathrm{U}}\rangle$ and $|\pm 1^{\mathrm{U}}\rangle$ is different for $p > 0.35$ and $p < 0.35$. For example, for $p = 0.39$, the $|0^{\mathrm{U}}\rangle$ state has a lower energy than $|\pm 1^{\mathrm{U}}\rangle$ state [Fig. 5(b)]; for $p = 0.25$, the $|0^{\mathrm{U}}\rangle$ state has a higher energy than $|\pm 1^{\mathrm{U}}\rangle$ state (Fig. S3). Actually, the level ordering is controlled by the positive and negative values of Δ, which depends on the parameters of CdSe core of DRs [26]. For the CdSe/CdS DRs with a larger CdSe dot, the $|0^{\mathrm{U}}\rangle$ state has a lower energy than $|\pm 1^{\mathrm{U}}\rangle$ state [26]. We can observe from Fig. 5(a) that $\Delta < 0$ corresponds to $p > 0.35$, and the polarization degrees tend to increase under the influence of the surface electrons; $\Delta > 0$ corresponds to $p < 0.35$, and the polarization degrees tend to decrease. Overall, the level ordering (or the positive and negative values of Δ) determines the degrees of polarization tending to increase or decrease under the influence of surface electrons.

It can be noticed from Fig. 5(b) that the polarization degrees increased from 0.39 to 0.50 is associated with the descending of $|0^{\mathrm{U}}\rangle$ level and the rising of $|\pm 1^{\mathrm{U}}\rangle$ level, and therefore the level spacing between $|0^{\mathrm{U}}\rangle$ and $|\pm 1^{\mathrm{U}}\rangle$ increases. In this case, the values of Δ are changed from -4.2 meV to -17.0 meV, and the population N of the $|0^{\mathrm{U}}\rangle$ state increases from 23.2% to 26.0%, while the population N of the $|\pm 1^{\mathrm{U}}\rangle$ state decreases from 20.3% to 14.7% (in Table 1). As a result, the emission probability of the 1D dipole $I_{1\mathrm{D}}$ increases from 57.9% to 66.5%, while the emission probability of the 2D dipoles $I_{2\mathrm{D}}$ decreases from 42.1% to 34.5% (in Table 1). Therefore, the level spacing determines the populations of the emitting states, and then controls the degrees of polarization.

Under the influence of surface electrons, the polarization degrees increased from 0.50 to 0.54 is associated with the descending of both $|0^{\mathrm{U}}\rangle$ and $|\pm 1^{\mathrm{U}}\rangle$ levels, but the $|0^{\mathrm{U}}\rangle$ level descends more than the $|\pm 1^{\mathrm{U}}\rangle$ level [Fig. 5(b)]. So, the level spacing between $|0^{\mathrm{U}}\rangle$ and $|\pm 1^{\mathrm{U}}\rangle$ increases. As a result, the population N of the $|0^{\mathrm{U}}\rangle$ state increases more than that of the $|\pm 1^{\mathrm{U}}\rangle$ state (in Table 1). Therefore, the surface electrons can increase the level spacing between $|0^{\mathrm{U}}\rangle$ and $|\pm 1^{\mathrm{U}}\rangle$, and then change the populations of the emitting states, and thus change the degrees of polarization.

Quantitative electrostatic force microscopy measurements showed that there are 2–3 electrons on single spher-

Table 1 Exciton fine structure and emission parameters for three different polarization degrees investigated.

p	η (meV)[a)]	Δ (meV)[b)]	$R_e f_{0^U}$[c)]	N_{0^U}[d)]	$2f_{\pm 1^L}$[c)]	$N_{\pm 1^L}$[d)]	$2f_{\pm 1^U}$[c)]	$N_{\pm 1^U}$[d)]	I_{1D}[e)]	I_{2D}[f)]
0.39	5.8	−4.2	55.0%	23.2%	0.22%	56.5%	44.8%	20.3%	57.9%	42.1%
0.5	5.8	−17.0	55.0%	26.0%	2.1%	59.3%	43.0%	14.7%	66.5%	34.5%
0.54	2.9	−21.3	55.0%	34.1%	5.2%	50.1%	39.9%	15.8%	67.8%	32.2%

[a)]Electron-hole exchange interaction; [b)]Net-splitting; [c)]Oscillator strengths and [d)]Populations of the various emitting levels $|0^U\rangle$, $|\pm 1^L\rangle$ and $|\pm 1^U\rangle$; [e)]Emission probability of the 1D dipole; [f)]Emission probability of the 2D dipoles.

ical CdSe/ZnS QD (the diameter of $\sim$ 6.5 nm) surface when QDs are in contact with ITO [40]. In our simulation, $\sim$ 4 electrons are considered to be on the surface of single DR, since the long CdSe/CdS rods (the length $\sim$ 30 nm and the width of $\sim$ 6 nm) should be able to hold more electrons on their surfaces. In addition, both the number and the distribution of surface electrons on the long CdSe/CdS rods may be random, which causes the heterogeneous influences on the degrees of polarization of single DRs, since the influence of surface electrons on the exciton properties depends on the distances between the surface electrons and the CdSe core [33, 34]. Therefore, the broadened histogram of polarization degrees may also originate from the heterogeneous influences of surface electrons on single DRs in the experiment. In addition, as mentioned above, the size of CdSe dots in CdSe/CdS DRs controls the level ordering of band-edge exciton fine structure, and further determines the degrees of polarization tending to increase or decrease under the influence of surface electrons. For the CdSe/CdS DRs with a larger CdSe dot, the degrees of polarization would tend to increase under the influence of surface electrons due to owning a lower $|0^U\rangle$ state. Homogeneous CdSe dots can make the degrees of polarization of single DRs keep similar changes under the influence of surface electrons. Therefore, the larger and homogeneous CdSe dots are necessary for DRs-based practical applications to avoid the broadening of polarization degrees.

3 Conclusions

In this paper, we investigated the influence of surface charges on the emission polarization properties of single DRs by measuring the emission polarization and analyzing the band-edge exciton fine structure. The histogram of polarization degrees of single DRs in ITO was found to be broadened under the influence of surface electrons. The calculation results show that the degrees of polarization trend to increase or decrease under the influence of surface electrons, which depends on the level ordering of the $|0^U\rangle$ and $|\pm 1^U\rangle$ states. The surface electrons can increase the level spacing between the $|0^U\rangle$ and $|\pm 1^U\rangle$ states and then change their populations, and thus change the degrees of polarization. Overall, the higher degrees of polarization are further increased and the lower polarization degrees are further decreased under the influence of surface electrons, so that the histogram is broadened from the middle to both sides. In addition, different numbers of surface electrons may randomly distribute on the long CdSe/CdS rods, which leads to the heterogeneous influences on single DRs causing the broadening of polarization degrees also. A more homogeneous DR samples should be synthesized to avoid the broadening of polarization degrees in practical applications. The insight into the influence of surface charges on the emission polarization properties of single DRs as well as the band-edge exciton fine structure is important for the DRs polarization-based applications.

4 Methods

4.1 Sample preparation

The CdSe/CdS DRs were fabricated by following a published synthetic method [63]. The length and the width of DRs are $\sim$ 30 nm and $\sim$ 6 nm, respectively, as determined by transmission electron microscopy (TEM) image in Fig. 1(a). The diameter of the CdSe core is $\sim$ 2.9 nm. The PL quantum yield of the DRs was measured to be 43%. Schematic representation of the sample preparation for single DRs in ITO is depicted in Fig. 1(c). Single DRs in toluene ($\sim 10^{-9}$ mol·L^{-1}) were spin-coated onto glass coverslip at 2000 rpm for 2 minutes, and then the ITO nanoparticles ($<$ 100 nm particle size, 30 wt.% in isopropanol, Sigma-Aldrich) were spin-coated onto individual DRs at 3000 rpm for 3 minutes. Through these processes, individual DRs are in contact with ITO nanoparticles. The samples were placed in vacuum at 315 K for 3 hours to remove the residual solvent. In addition, single DRs were prepared onto glass coverslip as a control experiment.

4.2 Single particle polarization microscopy

Scheme of the experimental setup for single particle polarization measurement is presented in Fig. 2(a). A rotating half-wave plate combined with a polarizing beam splitter was used for polarization detection in a confocal microscope. Single DRs were excited by a 485 nm picosecond pulsed diode laser (PDL808 PicoQuant), and the repeti-

tion frequency of laser was set at 5 MHz. The laser passed through a $\lambda/4$ wave-plate to form circular polarization light, and then was sent into a conventional inverted fluorescence microscope (IX71, Olympus) from its back side, reflected by a dichroic mirror (ZT488rdc, Chroma Technology Co.). An oil immersion objective lens (Olympus, 100×, 1.3 N.A.) was used to focus the laser beam onto the sample of the glass coverslip. The PL photons from single DRs were collected by the same objective lens and then passed through the dichroic mirror and an emission filter (ET500lp, Chroma Technology Co.). After that, the photons were focused onto a 100 μm pinhole for spatial filtering to reject out-of-focus photons. Two single photon detectors (PerkinElmer, SPCM-AQR-15) in a Hanbury-Brown and Twiss configuration were used to detect the PL photons. The signals from single photon detectors were recorded by a time-correlation single photon counting (TCSPC) data acquisition card (HydraHarp 400, PicoQuant) to obtain information about PL intensity trajectories, $g^{(2)}$ curves and decay curves. After distinguishing single DRs by $g^{(2)}$ method [55], the PL photons were subsequently sent to the rotating achromatic broadband half-wave plate (AHWP10M-600, 400–800 nm) combined with the broadband polarizing beamsplitter cube (Thorlabs, PBS121) to measure the polarization degrees of single DRs. The polarizing beamsplitter cube divided PL photons into its two components, and two additional single photon detectors are used to detect horizontal and vertical polarization photons, respectively. A piezo-scan stage (Piezosystem jena, Tritor 200/20 SG) with an active x–y–z feedback loop mounted on the inversion microscope was used to scan the DRs sample over the focus of the excitation spot. All measurements were performed at room temperature.

Acknowledgements The project was sponsored by the National Key Research and Development Program of China (Grant No. 2017YFA0304203), the National Natural Science Foundation of China (Grant Nos. 61527824, 61675119, 11434007, 61875109, and 61605104), PCSIRT (Grant No. IRT_17R70), 1331KSC and 111 project (Grant No. D18001).

Electronic Supplementary Materials Supplementary materials, i.e., the histograms of the PL intensities, fluorescence lifetime-intensity distribution (FLID), probability densities of on- and off-states, estimation of the parameters η and Δ, and the calculated band-edge exciton fine structure, are available in the online version of this article at https://doi.org/10.1007/s11467-019-0916-1 and are accessible for authorized users.

References

1. Z. G. Xiao, R. A. Kerner, L. F. Zhao, N. L. Tran, K. M. Lee, T. W. Koh, G. D. Scholes, and B. P. Rand, Efficient perovskite light-emitting diodes featuring nanometre-sized crystallites, *Nat. Photonics* 11(2), 108 (2017)
2. D. Han, M. Imran, M. Zhang, S. Chang, X. Wu, X. Zhang, J. Tang, M. Wang, S. Ali, X. Li, G. Yu, J. Han, L. Wang, B. Zou, and H. Zhong, Efficient light-emitting diodes based on in situ fabricated $FAPbBr_3$ nanocrystals: The enhancing role of the ligand-assisted reprecipitation process, *ACS Nano* 12(8), 8808 (2018)
3. V. I. Klimov, A. A. Mikhailovsky, S. Xu, A. Malko, J. A. Hollingsworth, C. A. Leatherdale, H. Eisler, and M. G. Bawendi, Optical gain and stimulated emission in nanocrystal quantum dots, *Science* 290(5490), 314 (2000)
4. D. C. Oertel, M. G. Bawendi, A. C. Arango, and V. Bulovic, Photodetectors based on treated CdSe quantum-dot films, *Appl. Phys. Lett.* 87(21), 213505 (2005)
5. G. C. Shan, Z. Q. Yin, C. H. Shek, and W. Huang, Single photon sources with single semiconductor quantum dots, *Front. Phys.* 9(2), 170 (2014)
6. W. S. Yang, B. W. Park, E. H. Jung, N. J. Jeon, Y. C. Kim, D. U. Lee, S. S. Shin, J. Seo, E. K. Kim, J. H. Noh, and S. I. Seok, Iodide management in formamidinium-lead-halide-based perovskite layers for efficient solar cells, *Science* 356(6345), 1376 (2017)
7. W. D. Sheng, M. Korkusinski, A. D. Guclu, M. Zielinski, P. Potasz, E. S. Kadantsev, O. Voznyy, and P. Hawrylak, Electronic and optical properties of semiconductor and graphene quantum dots, *Front. Phys.* 7(3), 328 (2012)
8. Y. Y. Fan, H. L. Liu, R. C. Han, L. Huang, H. Shi, Y. L. Sha, and Y. Q. Jiang, Extremely high brightness from polymer-encapsulated quantum dots for two-photon cellular and deep-tissue imaging, *Sci. Rep.* 5(1), 9908 (2015)
9. E. M. Thomas, S. Ghimire, R. Kohara, A. N. Anil, K. Yuyama, Y. Takano, K. G. Thomas, and V. Biju, Blinking suppression in highly excited CdSe/ZnS quantum dots by electron transfer under large positive Gibbs (free) energy change, *ACS Nano* 12(9), 9060 (2018)
10. G. Luo, Z. Z. Zhang, H. O. Li, X. X. Song, G. W. Deng, G. Cao, M. Xiao, and G. P. Guo, Quantum dot behavior in transition metal dichalcogenides nanostructures, *Front. Phys.* 12(4), 128502 (2017)
11. H. Huang, L. Polavarapu, J. A. Sichert, A. S. Susha, A. S. Urban, and A. L. Rogach, Colloidal lead halide perovskite nanocrystals: Synthesis, optical properties and applications, *NPG Asia Mater.* 8(11), e328 (2016)
12. H. Yuan, E. Debroye, E. Bladt, G. Lu, M. Keshavarz, K. P. F. Janssen, M. B. J. Roeffaers, S. Bals, E. H. Sargent, and J. Hofkens, Imaging heterogeneously distributed photo-active traps in perovskite single crystals, *Adv. Mater.* 30(13), 1705494 (2018)
13. Q. S. Chen, J. Wu, X. Ou, B. Huang, J. Almutlaq, A. A. Zhumekenov, X. Guan, S. Han, L. Liang, Z. Yi, J. Li, X. Xie, Y. Wang, Y. Li, D. Fan, D. B. L. Teh, A. H. All, O. F. Mohammed, O. M. Bakr, T. Wu, M. Bettinelli, H. Yang, W. Huang, and X. Liu, All-inorganic perovskite nanocrystal scintillators, *Nature* 561(7721), 88 (2018)
14. Q. B. Zeng, S. Chen, L. You, and R. Lu, Transport through a quantum dot coupled to two Majorana bound states, *Front. Phys.* 12(4), 127302 (2017)

15. A. Sitt, I. Hadar, and U. Banin, Band-gap engineering, optoelectronic properties and applications of colloidal heterostructured semiconductor nanorods, *Nano Today* 8(5), 494 (2013)
16. T. Kodanek, H. M. Banbela, S. Naskar, P. Adel, N. C. Bigall, and D. Dorfs, Phase transfer of 1- and 2-dimensional Cd-based nanocrystals, *Nanoscale* 7(45), 19300 (2015)
17. D. V. Talapin, R. Koeppe, S. Gotzinger, A. Kornowski, J. M. Lupton, A. L. Rogach, O. Benson, J. Feldmann, and H. Weller, Highly emissive colloidal CdSe/CdS heterostructures of mixed dimensionality, *Nano Lett.* 3(12), 1677 (2003)
18. I. Coropceanu, A. Rossinelli, J. R. Caram, F. S. Freyria, and M. G. Bawendi, Slow-injection growth of seeded CdSe/CdS nanorods with unity fluorescence quantum yield and complete shell to core energy transfer, *ACS Nano* 10(3), 3295 (2016)
19. M. Saba, S. Minniberger, F. Quochi, J. Roither, M. Marceddu, A. Gocalinska, M. V. Kovalenko, D. V. Talapin, W. Heiss, A. Mura, and G. Bongiovanni, Exciton-exciton interaction and optical gain in colloidal CdSe/CdS dot/rod nanocrystals, *Adv. Mater.* 21(48), 4942 (2009)
20. C. D. Sonnichsen, T. Kipp, X. Tang, and P. Kambhampati, Efficient optical gain in CdSe/CdS dots-in-rods, *ACS Photonics* 6(2), 382 (2019)
21. Y. Gao, V. D. Ta, X. Zhao, Y. Wang, R. Chen, E. Mutlugun, K. E. Fong, S. T. Tan, C. Dang, X. W. Sun, H. Sun, and H. V. Demir, Observation of polarized gain from aligned colloidal nanorods, *Nanoscale* 7(15), 6481 (2015)
22. M. Allione, A. Ballester, H. B. Li, A. Comin, J. L. Movilla, J. I. Climente, L. Manna, and I. Moreels, Two-photon-induced blue shift of core and shell optical transitions in colloidal CdSe/CdS quasi-type II quantum rods, *ACS Nano* 7(3), 2443 (2013)
23. A. Shabaev and A. L. Efros, 1D exciton spectroscopy of semiconductor nanorods, *Nano Lett.* 4(10), 1821 (2004)
24. N. Le Thomas, E. Herz, O. Schops, U. Woggon, and M. V. Artemyev, Exciton fine structure in single CdSe nanorods, *Phys. Rev. Lett.* 94(1), 016803 (2005)
25. Y. Louyer, L. Biadala, J. B. Trebbia, M. J. Fernee, P. Tamarat, and B. Lounis, Efficient biexciton emission in elongated CdSe/ZnS nanocrystals, *Nano Lett.* 11(10), 4370 (2011)
26. S. Vezzoli, M. Manceau, G. Lemenager, Q. Glorieux, E. Giacobino, L. Carbone, M. De Vittorio, and A. Bramati, Exciton fine structure of CdSe/CdS nanocrystals determined by polarization microscopy at room temperature, *ACS Nano* 9(8), 7992 (2015)
27. J. Planelles, F. Rajadell, and J. I. Climente, Electronic origin of linearly polarized emission in CdSe/CdS dot-in-rod heterostructures, *J. Phys. Chem. C* 120(48), 27724 (2016)
28. I. Hadar, G. B. Hitin, A. Sitt, A. Faust, and U. Banin, Polarization properties of semiconductor nanorod heterostructures: From single particles to the ensemble, *J. Phys. Chem. Lett.* 4(3), 502 (2013)
29. B. T. Diroll, A. Koschitzky, and C. B. Murray, Tunable optical anisotropy of seeded CdSe/CdS nanorods, *J. Phys. Chem. Lett.* 5(1), 85 (2014)
30. I. Angeloni, W. Raja, A. Polovitsyn, F. De Donato, R. P. Zaccaria, and I. Moreels, Band-edge oscillator strength of colloidal CdSe/CdS dot-in-rods: Comparison of absorption and time-resolved fluorescence spectroscopy, *Nanoscale* 9(14), 4730 (2017)
31. J. Müller, J. M. Lupton, A. L. Rogach, J. Feldmann, D. V. Talapin, and H. Weller, Monitoring surface charge movement in single elongated semiconductor nanocrystals, *Phys. Rev. Lett.* 93(16), 167402 (2004)
32. J. Müller, J. M. Lupton, A. L. Rogach, J. Feldmann, D. V. Talapin, and H. Weller, Monitoring surface charge migration in the spectral dynamics of single CdSe/CdS nanodot/nanorod heterostructures, *Phys. Rev. B* 72(20), 205339 (2005)
33. S. H. Lohmann, C. Strelow, A. Mews, and T. Kippe, Surface charges on CdSe-dot/CdS-rod nanocrystals: Measuring and modeling the diffusion of exciton-fluorescence rates and energies, *ACS Nano* 11(12), 12185 (2017)
34. S. H. Lohmann, P. Harder, F. Bourier, C. Strelow, A. Mews, and T. Kipp, Influence of interface-driven strain on the spectral diffusion properties of core/shell CdSe/CdS dot/rod nanoparticles, *J. Phys. Chem. C* 123(8), 5099 (2019)
35. M. J. Fernée, B. Littleton, T. Plakhotnik, H. Rubinsztein-Dunlop, D. E. Gomez, and P. Mulvaney, Charge hopping revealed by jitter correlations in the photoluminescence spectra of single CdSe nanocrystals, *Phys. Rev. B* 81(15), 155307 (2010)
36. M. J. Fernée, T. Plakhotnik, Y. Louyer, B. N. Littleton, C. Potzner, P. Tamarat, P. Mulvaney, and B. Lounis, Spontaneous spectral diffusion in CdSe quantum dots, *J. Phys. Chem. Lett.* 3(12), 1716 (2012)
37. K. T. Early, P. K. Sudeep, T. Emrick, and M. D. Barnes, Polarization-driven stark shifts in quantum dot luminescence from single CdSe/oligo-PPV nanoparticles, *Nano Lett.* 10(5), 1754 (2010)
38. T. Ihara and Y. Kanemitsu, Spectral diffusion of neutral and charged exciton transitions in single CdSe/ZnS nanocrystals due to quantum-confined stark effect, *Phys. Rev. B* 90(19), 195302 (2014)
39. D. Braam, A. Molleken, G. M. Prinz, C. Notthoff, M. Geller, and A. Lorke, Role of the ligand layer for photoluminescence spectral diffusion of CdSe/ZnS nanoparticles, *Phys. Rev. B* 88(12), 125302 (2013)
40. S. E. Yalcin, B. Q. Yang, J. A. Labastide, and M. D. Barnes, Electrostatic force microscopy and spectral studies of electron attachment to single quantum dots on indium tin oxide substrates, *J. Phys. Chem. C* 116(29), 15847 (2012)
41. S. Y. Jin, N. H. Song, and T. Q. Lian, Suppressed blinking dynamics of single QDs on ITO, *ACS Nano* 4(3), 1545 (2010)

42. H. Cheng, C. Yuan, J. Wang, T. Lin, J. Shen, Y. Hung, J. Tang, and F. Tseng, Modification of photon emission statistics from single colloidal CdSe quantum dots by conductive materials, *J. Phys. Chem. C* 118(31), 18126 (2014)
43. B. Li, G. Zhang, Z. Wang, Z. Li, R. Chen, C. Qin, Y. Gao, L. Xiao, and S. Jia, Suppressing the fluorescence blinking of single quantum dots encased in N-type semiconductor nanoparticles, *Sci. Rep.* 6(1), 32662 (2016)
44. Z. J. Li, G. F. Zhang, B. Li, R. Y. Chen, C. B. Qin, Y. Gao, L. T. Xiao, and S. T. Jia, Enhanced biexciton emission from single quantum dots encased in N-type semiconductor nanoparticles, *Appl. Phys. Lett.* 111(15), 153106 (2017)
45. K. T. Early, K. D. McCarthy, M. Y. Odoi, P. K. Sudeep, T. Emrick, and M. D. Barnes, Linear dipole behavior in single CdSe-oligo(phenylene vinylene) nanostructures, *ACS Nano* 3(2), 453 (2009)
46. G. F. Zhang, Y. G. Peng, H. Q. Xie, B. Li, Z. J. Li, C. G. Yang, W. L. Guo, C. B. Qin, R. Y. Chen, Y. Gao, Y. J. Zheng, L. T. Xiao, and S. T. Jia, Linear dipole behavior of single quantum dots encased in metal oxide semiconductor nanoparticles films, *Front. Phys.* 14(2), 23605 (2019)
47. A. P. Litvin, I. V. Martynenko, F. Purcell-Milton, A. V. Baranov, A. V. Fedorov, and Y. K. Gun'ko, Colloidal quantum dots for optoelectronics, *J. Mater. Chem. A* 5(26), 13252 (2017)
48. Y. Jiang, S. Cho, and M. Shim, Light-emitting diodes of colloidal quantum dots and nanorod heterostructures for future emissive displays, *J. Mater. Chem. C* 6(11), 2618 (2018)
49. L. Meng, C. Yang, J. Meng, Y. Wang, Y. Ge, Z. Shao, G. Zhang, A. L. Rogach, and H. Zhong, In-situ fabricated anisotropic halide perovskite nanocrystals in polyvinylalcohol nanofibers: Shape tuning and polarized emission, *Nano Res.* 12(6), 1411 (2019)
50. T. Ihara, R. Sato, T. Teranishi, and Y. Kanemitsu, Delocalized and localized charged excitons in single CdSe/CdS dot-in-rods revealed by polarized photoluminescence blinking, *Phys. Rev. B* 90(3), 035309 (2014)
51. F. Hu, B. Lv, C. Yin, C. Zhang, X. Wang, B. Lounis, and M. Xiao, Carrier multiplication in a single semiconductor nanocrystal, *Phys. Rev. Lett.* 116(10), 106404 (2016)
52. G. C. Yuan, D. E. Gomez, N. Kirkwood, K. Boldt, and P. Mulvaney, Two mechanisms determine quantum dot blinking, *ACS Nano* 12(4), 3397 (2018)
53. B. Li, H. Huang, G. Zhang, C. Yang, W. Guo, R. Chen, C. Qin, Y. Gao, V. P. Biju, A. L. Rogach, L. Xiao, and S. Jia, Excitons and biexciton dynamics in single $CsPbBr_3$ perovskite quantum dots, *J. Phys. Chem. Lett.* 9(24), 6934 (2018)
54. H. Yuan, E. Debroye, G. Caliandro, K. P. Janssen, J. van Loon, C. E. Kirschhock, J. A. Martens, J. Hofkens, and M. B. Roeffaers, Photoluminescence blinking of single-crystal methylammonium lead iodide perovskite nanorods induced by surface traps, *ACS Omega* 1(1), 148 (2016)
55. B. Li, G. Zhang, C. Yang, Z. Li, R. Chen, C. Qin, Y. Gao, H. Huang, L. Xiao, and S. Jia, Fast recognition of single quantum dots from high multi-exciton emission and clustering effects, *Opt. Express* 26(4), 4674 (2018)
56. H. Zang, P. K. Routh, Y. Huang, J. S. Chen, E. Sutter, P. Sutter, and M. Cotlet, Nonradiative energy transfer from individual CdSe/ZnS quantum dots to single-layer and few-layer tin disulfide, *ACS Nano* 10(4), 4790 (2016)
57. W. He, C. Qin, Z. Qiao, Y. Gong, X. Zhang, G. Zhang, R. Chen, Y. Gao, L. Xiao, and S. Jia, In situ manipulation of fluorescence resonance energy transfer between quantum dots and monolayer graphene oxide by laser irradiation, *Nanoscale* 11(3), 1236 (2019)
58. C. Lethiec, J. Laverdant, H. Vallon, C. Javaux, B. Dubertret, J. M. Frigerio, C. Schwob, L. Coolen, and A. Maitre, Measurement of three-dimensional dipole orientation of a single fluorescent nanoemitter by emission polarization analysis, *Phys. Rev. X* 4(2), 021037 (2014)
59. A. L. Efros, M. Rosen, M. Kuno, M. Nirmal, D. J. Norris, and M. Bawendi, Band-edge exciton in quantum dots of semiconductors with a degenerate valence band: Dark and bright exciton states, *Phys. Rev. B* 54(7), 4843 (1996)
60. A. Sihvola, Dielectric polarization and particle shape effects, *J. Nanomater.* 2007, 45090 (2007)
61. J. S. Kamal, R. Gomes, Z. Hens, M. Karvar, K. Neyts, S. Compernolle, and F. Vanhaecke, Direct determination of absorption anisotropy in colloidal quantum rods, *Phys. Rev. B* 85(3), 035126 (2012)
62. S. L. Chuang and C. S. Chang, $\boldsymbol{K}\cdot\boldsymbol{P}$ method for strained Wurtzite semiconductors, *Phys. Rev. B* 54(4), 2491 (1996)
63. L. Carbone, C. Nobile, M. De Giorgi, F. D. Sala, G. Morello, P. Pompa, M. Hytch, E. Snoeck, A. Fiore, I. R. Franchini, M. Nadasan, A. F. Silvestre, L. Chiodo, S. Kudera, R. Cingolani, R. Krahne, and L. Manna, Synthesis and micrometer-scale assembly of colloidal CdSe/CdS nanorods prepared by a seeded growth approach, *Nano Lett.* 7(10), 2942 (2007)